International Journal of Industrial Electronics, Control and Optimization © 2020 IECO
Vol. 3, No. 3, pp. 235-247, July (2020)

Voltage Unbalancing Reduction in a Stand-Alone AC-DC Hybrid Microgrid Based on Floating Compensation Reference

Seyed Hossein Tabatabaei[1], Hussein Eliasi[2,†], and Hamid Reza Najafi[3]

[1,2,3]Faculty of Electrical and Computer Engineering, University of Birjand, Birjand, Iran

ABSTRACT

A hybrid AC-DC microgrid consists of an AC and a DC subgrid which are connected to each other through an interlinking converter (IC). The main function of an IC under islanded conditions is to transfer power between the two subgrids. In this paper, a scheme is presented to reduce the voltage unbalance factor in a hybrid AC-DC microgrid by using the free capacity of the IC. The free capacity of this converter is determined based on the current passing through each leg, and the amount of voltage unbalance compensation on the AC side of the microgrid is then obtained. The reference current of voltage unbalance compensation is calculated by using the positive, negative, and zero sequence components of the voltage of IC terminals. The total reference current is obtained by adding the reference current of voltage unbalance compensation and the current calculated for power transfer. Furthermore, a proportional-resonant (PR) controller is used in the control system of the four-leg inverter. Therefore, the reference current is properly tracked by the power stage of the inverter. Simulation results verify the accuracy of the proposed scheme under different conditions.

Article Info

Keywords:
Hybrid AC-DC microgrid, Interlinking converter, Power quality, Voltage unbalance.

Article History:
Received 2019-09-12
Accepted 2020-01-12

NOMENCLATURE

u_{abc}	Voltage of the AC subgrid
u_{CB}	Voltage of the capacitor C_B
u_{DC}	Voltage of the DC subgrid
$u_{\max}, u_{\min}$	Maximum and minimum of allowable value of DC subgrid voltage
u_o	Output voltage of the boost converter
U_{AC}	Reference voltage of the AC subgrid
u_{LL}^{abc}	Line to line voltage of the AC subgrid
u_e	Effective voltage of the ac subgrid
u_{rms}^{012}	Effective voltage of the zero, positive and negative voltage of the AC subgrid
d	Duty Cycle of the buck/boost converter
i_{dc}	Inductance current of the buck/boost converter
i_{IC}^{abcn}	Output current of the four-leg inverter
i_o	Output Current of the boost converter
i_{abc}	Line Current of the AC subgrid
$I_{\alpha\beta}^{*}$	Reference current of the IC in αβ reference frame for power transfer between two subgrids
I_R	Maximum value of the allowable current of the each leg in four-leg inverter
I_N	Maximum value of the effective current between *abc* branches in the four-leg inverter
I_M	Maximum value of the effective current between *abcn* branches in the four-leg inverter

†Corresponding Author: h_eliasi@birjand.ac.ir
Tel: +98-9122454027
Faculty of Electrical and Computer Engineering, University of Birjand, Birjand, Iran.

ω	Reference angular frequency of the AC subgrid
f	Frequency of the AC subgrid
f_{max}, f_{min}	Maximum and minimum of allowable value of AC subgrid frequency
UR_0, UR_2	Compensation references of the negative and zero sequence voltage of the AC subgrid
UF_0, UF_2	Zero and negative unbalance indexes
P_{IC}, Q_{IC}	Actual active and reactive power transferred between two subgrids

I. INTRODUCTION

According to the IEEE standards, a microgrid is a local network that is composed of distributed energy sources (DERs) and loads and can continue to work either in grid-connected or in islanded modes of operation. A DER can be either an energy generation source or an energy storage source [1]. Microgrids can be categorized in three main groups from structural and operational points of view. From a structural point of view, microgrids are classified as AC, DC, and hybrid AC-DC microgrids [2]-[5]. On the other hand, from an operational point of view, microgrids can be categorized as grid-connected, islanded, and a transient state between these two states [6]-[9].

Among various kinds of microgrids, the hybrid AC-DC microgrid is an effective way for proper and efficient exploitation of DGs, as well as AC and DC loads. A hybrid microgrid is composed of an AC subgrid, a DC subgrid, and an interlinking converter which connects these two subgrids [10], [11]. A hybrid microgrid has the advantages of both AC and DC subgrids. Due to the decrease in the number of stages of electronic power converters in this microgrid and consequently a decrease in the loss, the efficiency of this microgrid increases. However, its control and utilization is much more complicated than AC and DC subgrids. Due to the many advantages of hybrid microgrids, they can be considered as the future distribution networks.

In various papers related to AC-DC hybrid microgrids, published up until now, different strategies have been proposed for IC. When the microgrid is operated in grid-connected mode, the IC has the duty of voltage stabilization of the DC sub-grid and the power control [12]. If the microgrid is operated in islanded mode, according to the type of the control of AC and DC sub-grids, the IC has to control a DC sub-grid, an AC sub-grid or the output power [13]. In [14], four operation modes are defined for the IC:

- Both the AC and DC subgrids are under under-load conditions; in this mode the IC is off.
- Both the AC and DC subgrids are under full-load conditions; in this mode the IC is off.
- The AC subgrid is under under-load conditions and the DC subgrid is under full-load or over-load conditions; in this mode, the power is transferred from the AC subgrid to the DC subgrid by the IC.
- The AC subgrid is under full-load or over-load conditions and the DC subgrid is under under-load conditions; in this mode, the power is transferred from the DC subgrid to the AC subgrid by the IC.

Considering the four modes discussed for the hybrid microgrid [14], it can be concluded that the IC has free capacity during the most hours of the day. Therefore, in addition to transferring power between two subgrids, the capacity of IC can be used for other auxiliary purposes as well.

One of the most important factors that must be taken into account in the initial design of a microgrid is supplying the power required by the loads with proper and standard quality [15], particularly in the islanded mode. However, the improvement of the power quality indices in hybrid microgrids has rarely been taken into account so far. Voltage unbalance is one of the most common power quality phenomena which cause interference in the operation of equipment especially in induction machines [16]. The presence of single-phase loads in three phase networks is one of the main causes of voltage unbalance in three phase four-wire distribution networks. There are several different ways to compensate voltage unbalance in a distribution network. One approach is to use a custom power equipment such as parallel active power filter [17], UPQC and D-STATCOM [18], [19]. However, this approach is not economical. In another method, the interfacing converter between DG and network can be employed to compensate voltage unbalance. As an example, [20]-[22] use the interfacing converter to compensate voltage unbalance in a three-phase three-wire system. However, voltage unbalance compensation through the interfacing converter reduces the power injection capability. In [23], [24] the series converter has been used to improve voltage quality in the hybrid AC-DC microgrid. However, the use of the series converter is a costly investment due to the existence of the transformer. In [25], [26] the elimination of power oscillations is investigated in conditions where several ICs are in parallel. Despite, this is accompanied by a reduction in transmission power and requires the sum of the entire IC's currents.

While, distribution networks are mainly four-wire networks with a null wire, Nevertheless, far too little attention has been paid to the power quality problems in these grids. In this paper, since the AC subgrid is a three phase four-wire system, the IC is composed of a four-leg converter on the AC side and a buck/boost converter on the DC side. Using the buck/boost converter makes it possible to change the voltage levels of the AC and DC subgrids [27].

The scientific contribution of this paper, which has not been taken into account so far, can be stated as follows:

- Using IC for improving the power quality indices on the AC side of the sub-grid, particularly, for improving the voltage unbalance indices,
- Determining the reference value of unbalance indices of zero and negative sequence voltages in an adaptive

manner and based on the nominal capacity and the capacity used in IC converter,

- Increasing the compensation capacity of the IC converter by means of imaginary admittance.

Next in this paper, first the way in which the microgrid is controlled is described. This section includes the control approaches of the AC and the DC microgrids as well as the IC. Dynamic modeling of the IC and design of its controllers are presented in section 2. And the way the reference current is generated based on the zero and negative sequence is described in section 3. One of the factors that must be taken into account in determining the amount of compensation is the maximum current that can pass through each leg of the IC. In this paper, this is done by changing the value of compensation reference and it is described in section (3-2). Furthermore, in section 4, several modes are defined for investigating the performance of the proposed scheme and the results of simulation are shown. Finally, section 5 concludes the paper.

II. Modeling and Controlling the Hybrid AC-DC Microgrid

Fig. 1 shows a hybrid AC-DC microgrid in islanded mode. In all sources of the microgrid, droop control is used to adjust the voltage and frequency. Therefore, in both the AC and DC subgrids, all the distributed sources and loads can be integrated and represented as an equivalent system with a source and a load [28]. The subgrids can be connected to each other through one or more ICs.

Depending on the structure and conditions of the hybrid subgrid, the IC can perform three different tasks: 1-Adjusting the voltage of the DC subgrid, 2-Adjusting the voltage and frequency of the AC microgrid, and 3-Controlling the power transferred between two subgrids [13]. Under islanded conditions, controlling the power transferred between two subgrids is of great importance, however, considering the importance and sensitivity of the AC and DC loads in microgrids, controlling the voltage (and frequency) of subgrids can also be put higher priority. In this paper, controlling the power transferred between two subgrids is considered to be the main duty of the IC.

A. Controlling the DC Subgrid

The way in which an equivalent source is determined for several distributed generation sources based on their rated powers and the droop coefficients of their controllers has been described in [28]. Therefore in this paper, instead of considering several distributed generation sources, a source together with a boost converter and a droop controller have been used, as shown in fig. 2. Eq. (1) shows the droop control of voltage based on the output current of the boost converter:

$$u_O = U_O^{ref} - R_d \times i_o \tag{1}$$

where, u_o is the voltage of the converter, U_O^{ref} is the reference voltage of the converter under no-load conditions, R_d is the droop coefficient and i_o is the output current of the converter. Based on the data presented in Table I, the way the system voltage changes according to the output current of the converter is shown in Fig. 3. It is obvious that if the resistance of the linking lines between the load and source is taken into consideration, the voltage across the load will be less than the value determined.

B. Controlling the AC Subgrid

Fig. 4 shows the AC subgrid with its control system. In the AC microgrid, the droop control approach is used for determining the reference frequency and voltage. Eq. (2) shows the way in which the reference frequency and voltage are determined based on the active and reactive power of the load [29]:

$$\begin{aligned} \omega &= \omega^{ref} - m \times P_{load} \\ U_{AC} &= U_{AC}^{ref} - n \times Q_{load} \end{aligned} \tag{2}$$

where, ω and U_{AC} are the reference angular frequency and voltage of the converter, ω^{ref} and U_{AC}^{ref} are the reference angular frequency and voltage of the subgrid under no-load conditions, m and n are the droop coefficients of the frequency and voltage of the subgrid, and finally P_{load} and Q_{load} are the consumed active and reactive power of the AC subgrid, respectively.

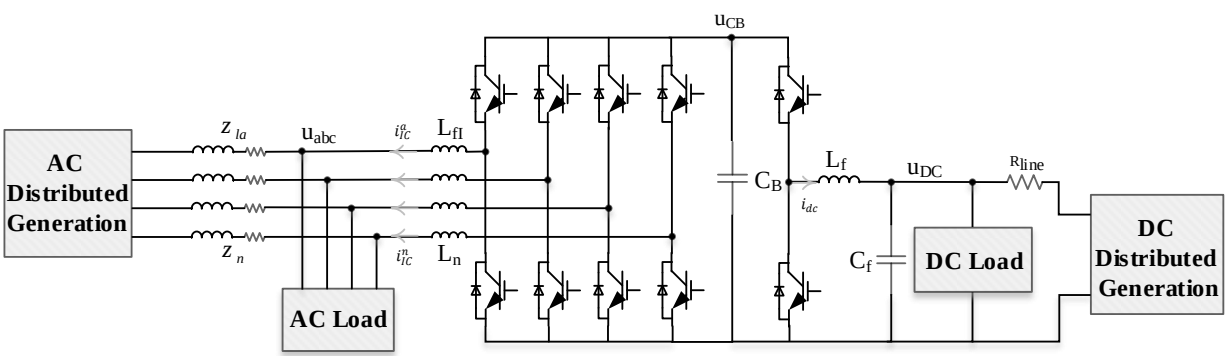


Fig. 1. Structure of hybrid AC-DC microgrid

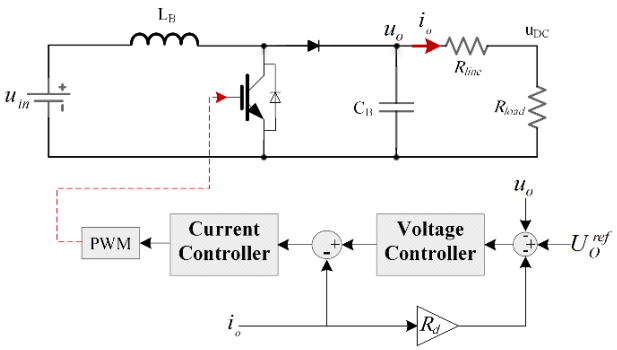


Fig. 2. A simple structure of the DC subgrid

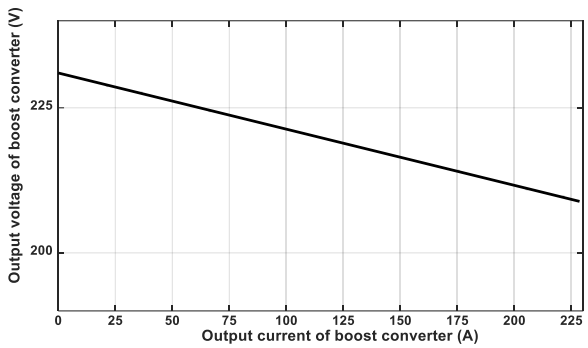


Fig. 3. The droop curve of voltage versus the current of the boost converter

Table I

THE CHARACTERISTICS OF THE DC SUBGRID AND THE BOOST CONVERTER

The input voltage of the converter	80-150 V	The rated voltage of the DC subgrid	220 V
The switching frequency of the converter	10 kHz	The reference current under no-load conditions (U_{DC}^{ref})	231 V
Inductance of the converter (Ls)	1 mH	Droop coefficient (R_d)	0.0968
The capacitor of the converter (C)	1 mF	The maximum power of the subgrid (P_{DC}^{max})	50 kW

C. Controlling the Interlinking Converter

The way in which the interlinking converter in a hybrid microgrid is controlled is of great importance. This converter acts as an inverter when it transfers power from the DC subgrid to the AC subgrid, and it will be similar to an active rectifier when the power is transferred in the opposite direction [30]. Considering the fact that the main task of this converter is to transfer power between two subgrids, a more comprehensive relationship is needed for calculating the reference power of this converter. To do this, first the frequency of the AC subgrid and the voltage of the DC subgrid are normalized in the interval between 0 and -1 [14]:

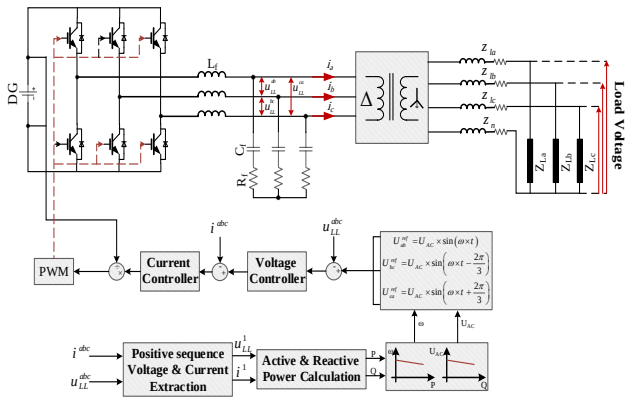


Fig. 4. The structure and the control system of the AC subgrid

$$f_{pu}^{AC}=\frac{f-f_{max}}{f_{max}-f_{min}}$$
$$u_{pu}^{DC}=\frac{u_{DC}-u_{max}}{u_{max}-u_{min}} \quad (3)$$

where, f and u_{DC} are the frequency of the AC subgrid and the load voltage of the DC subgrid, and the subscripts *max* and *min* represent the maximum and minimum values of the frequency and voltage, respectively. Due to the decrease in loss, the IC will enter the system only if the values of f_{pu}^{AC} and u_{pu}^{DC} are smaller than a certain value. Therefore, a droop relationship as (4) and (5) can be considered for calculating the power transferred between the subgrids [14]:

$$P_{ICa}=\begin{cases}0 & 0<f_{pu}^{AC}\le f_T\\ -k_a\left(f_{pu}^{AC}-f_T\right) & f_B\le f_{pu}^{AC}\le f_T\\ P_T & -1\le f_{pu}^{AC}<f_B\end{cases}$$
$$P_{ICb}=\begin{cases}0 & 0<u_{pu}^{DC}\le u_T\\ -k_b\left(u_{pu}^{DC}-u_T\right) & v_B\le u_{pu}^{DC}\le u_T\\ P_T & -1\le u_{pu}^{DC}<u_B\end{cases} \quad (4)$$

$$P_{IC}=P_{ICa}-P_{ICb} \quad (5)$$

where, P_{ICa} and P_{ICb} are the power demanded by the AC and DC subgrids, P_{IC} is the actual power transferred by the IC and P_T is the maximum transferable power which is basically limited by the nominal capacity of the IC. In Fig. 5, the other parameters of Eq. 4 are properly shown.

Reactive power exchange takes places only when the active power is transferred from the DC subgrid to the AC subgrid. This is because the DC subgrid does not require reactive power [31]. Therefore, the reference active power is calculated using Eq. (6):

$$Q_{IC}=\begin{cases}k_q\left(u_e-u_{ac}^n\right) & P_{IC}\ge 0\\ 0 & P_{IC}<0\end{cases} \quad (6)$$

$$u_e=\sqrt{\left(u_{rms}^1\right)^2+\left(u_{rms}^2\right)^2+\frac{\left(u_{rms}^0\right)^2}{2}} \quad (7)$$

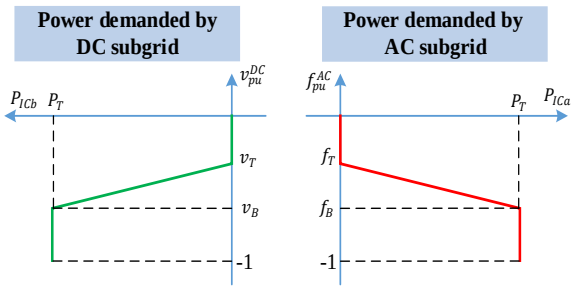


Fig. 5. The droop curve for calculating the power demand of the subgrid

where, $\boldsymbol{k_q}$ is the droop slope of the voltage control, $\boldsymbol{u_e}$ is the effective voltage of the IC terminals [32], $\boldsymbol{u_{ac}^n}$ is the voltage of IC terminals under nominal conditions, $\boldsymbol{u_{rms}^1}$, $\boldsymbol{u_{rms}^2}$, and $\boldsymbol{u_{rms}^0}$ are the effective values of the positive, negative, and zero sequences of the voltage of the IC terminals, respectively. Finally, the reference currents in αβ reference frame are calculated as shown by Eq. (8):

$$\begin{bmatrix} i_\alpha^{ref} \\ i_\beta^{ref} \end{bmatrix} = \frac{1}{\left(u_\alpha^1\right)^2+\left(u_\beta^1\right)^2}\begin{bmatrix} u_\alpha^1 & u_\beta^1 \\ u_\beta^1 & -u_\alpha^1 \end{bmatrix}\begin{bmatrix} P_{IC} \\ Q_{IC} \end{bmatrix} \tag{8}$$

D. Designing the Controller of the Interlinking Converter

To design the controller, the IC is divided into two parts; a buck/boost converter which is responsible for adjusting the voltage of the capacitor C_B, and a four-leg inverter which acts as a controlled current source. The control system of the buck/boost converter is composed of a voltage control loop and a current control loop. The inner loop which adjusts the duty cycle must have a higher responding speed than the outer voltage control loop. This is necessary for making the interference between two loops insignificant. On the other hand, since the four-leg inverter also acts as a current source, its control needs to be faster than that of the voltage control loop of the buck/boost converter. Thus, the effect of interference between two converters will be insignificant.

1) Designing the Controller of the Buck/Boost Converter

Fig. 6 shows the buck/boost converter and the effective elements in its modeling. Using the averaging technique in state space [33], the transfer functions (9) and (10) are obtained for the system shown in Fig. 6:

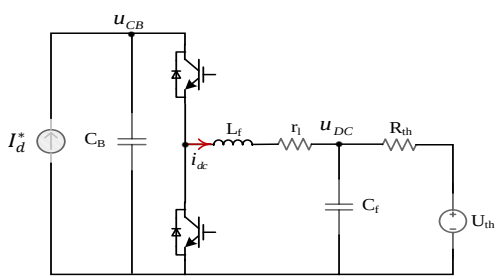


Fig. 6. A simple model of the DC subgrid, the buck/boost converter and the four- leg inverter

$$\hat{i}_{dc}(s)=G_1(s)\hat{d}(s)+H_1\hat{i}_d^*(s)+F_1(s)\hat{u}_{th}(s) \tag{9}$$

$$\hat{u}_{CB}(s)=G_2(s)\hat{d}(s)+H_2\hat{i}_d^*(s)+F_2(s)\hat{u}_{th}(s) \tag{10}$$

where,

$$\begin{aligned} &G_1(s)=\frac{A}{den} \quad H_1(s)=\frac{B}{den} \quad F_1(s)=\frac{C}{den} \\ &G_2(s)=\frac{E}{den} \quad H_2(s)=\frac{J}{den} \quad F_2(s)=\frac{I}{den} \end{aligned} \tag{11}$$

$$den=C_BC_fL_fR_{th}s^3+\left(C_BC_fr_lR_{th}+C_BL_f\right)s^2+\left(C_Br_l+C_BR_{th}+C_fR_{th}D^2\right)s+D^2$$

$$A=-\left(DI_{DC}-C_BU_{CB}s\right)\left(C_fR_{th}s+1\right)$$

$$B=D\left(C_fR_{th}s+1\right)$$

$$C=-C_Bs$$

$$E=-(C_fI_{DC}L_fR_{th}s^2+\left(C_fI_{DC}r_lR_{th}+C_fU_{CB}R_{th}D+I_{DC}L_f\right)s+I_{DC}\left(R_{th}+r_l\right)+DU_{CB})$$

$$J=C_fL_fR_{th}s^2+(C_fr_lR_{th}+L_f)s+r_l+R_{th}$$

$$I=D$$

$$I_{DC}=\frac{I_d^*}{D}$$

$$U_{CB}=\frac{u_{th}}{D}+\frac{I_d^*\left(r_l+R_{th}\right)}{D^2}$$

in the equations above, the symbol '^' represents slight changes in the variable, and I_{DC}, U_{CB}, and D are the current of the inductance L_f, the voltage of the capacitor C_B, and the duty cycle of the converter in the operating point, respectively. According to the data presented in Table II, the frequency characteristic curve of Eq. (11) is shown for the two cases in which the active power transferred between the AC and DC subgrids is at its maximum allowable value. Since the system must be stable in all its operating points, the controller needs to be designed for the worst conditions that might exist. In the system of interest, the worst conditions take place when the maximum power is transferred from the AC subgrid to the DC subgrid. This appears as a phase lag in the transfer function G_1 (the red line) in Fig. 7.

The control scheme of interest for controlling the voltage and current is shown in Fig. 8. Two PI controllers are used for adjusting the voltage and current. The inner loop is responsible for controlling the current and the outer loop is responsible for controlling the voltage. By adjusting the coefficients of the controller for the worst operating point of the buck/boost controller according to Table II, the frequency response of the closed loop transfer function of the inductance current and the capacitor (C_B) voltage to its effective inputs are obtained for two operating points of $I_d^* = \pm 22$ A, as shown in Fig. 9.

It can be seen from the closed loop transfer functions in Fig. 9 that the bandwidth of the transfer function u_{CB}/U_{CB}^{ref}

is much smaller than that of i_{dc}/i_{dc}^{ref}. This means that the

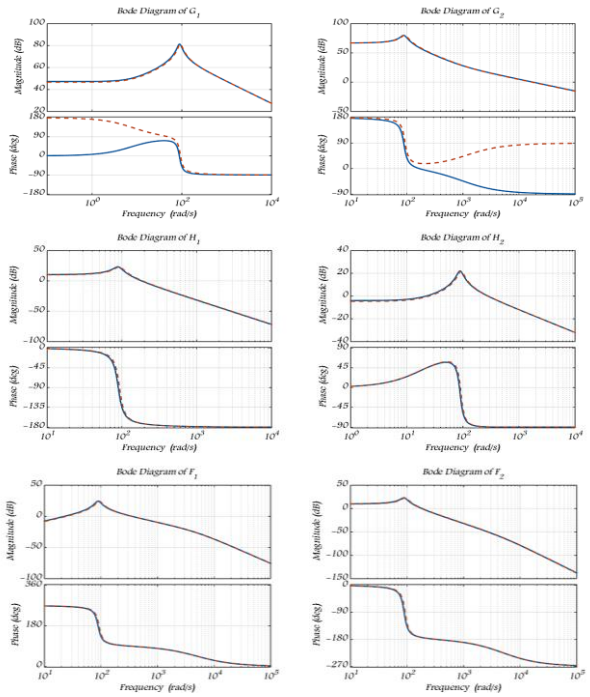


Fig. 7. The frequency response of the transfer function (11) in two operating points (the blue line at $I_d^* = -22\ A$ and the red line at $I_d^* = 22\ A$)

responding speed of the voltage loop is lower than that of the current control loop.

2) Designing the Controller of the Four-leg Inverter

The four-leg inverter in fact plays the role of a controlled current source. The PWM modulation approach makes it possible for the power part in the inverter to appear in modeling as a gain proportional to the voltage of the DC link and the delays caused by sampling and pulse width modulation ($T_{delay} = 0.75/f_{sw}$) [35]. Since the system contains a zero sequence component, so we convert it to three independent systems in the αβ0 frame using Clark's transformation. Fig. 10 shows the model extracted for the four-leg inverter in αβ0 frame [34] for current controlled mode. A proportional-resonant (PR) controller has been selected because it properly tracks the sinusoidal signals [35]. Eq. (12) shows the transfer function of this controller:

$$G_C(s) = k_p + \frac{2k_i\omega_r s}{s^2 + 2\omega_r s + \omega_0^2} \qquad (12)$$

where in this equation, k_p, k_i, ω_r and ω_0 are the proportional coefficient, integral coefficient, the bandwidth, and the resonance frequency of the controller, respectively. Theoretically, the coefficients of the controller need to be as large as possible. However, existence of delays in the PWM and computation causes the selected ranges for the control coefficients to be small. The way in which the controller coe-

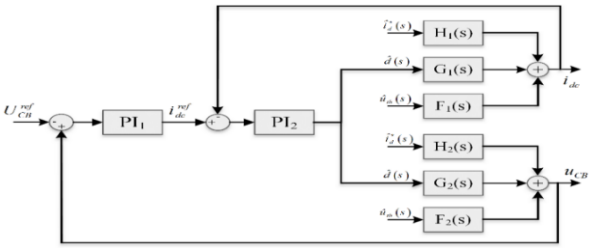


Fig. 8. The block diagram of the buck/boost converter

Table II

THE CHARACTERISTICS OF THE BUCK/BOOST CONVERTER FOR DESIGNING THE CONTROL SYSTEM

Thevenin equivalent voltage (u_{th})	220 V
Thevenin equivalent resistance (R_{th})	0.03 Ω
The capacitance of capacitors (C_B)	4000 µF
The inductance (L_f)	3 mH
The resistance of the inductor (r_l)	0.01 Ω
The value of I_d^* for maximum power exchange	$\pm 22\ A$
Voltage controller (PI_1)	$k_{p1} = 1 \quad k_{i1} = 10$
Current controller (PI_2)	$k_{p2} = 0.2 \quad k_{i2} = 5$

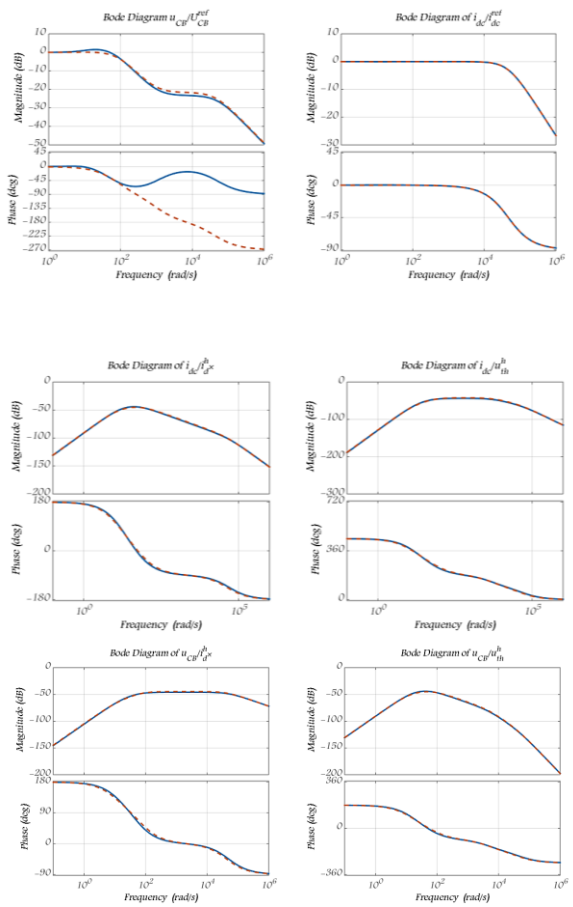


Fig. 9. The frequency response of the closed loop system of the buck/boost converter (the blue line a $\mathbf{I_d^* = 22\ A}$ t and the red line at $\mathbf{I_d^* = -22\ A}$)

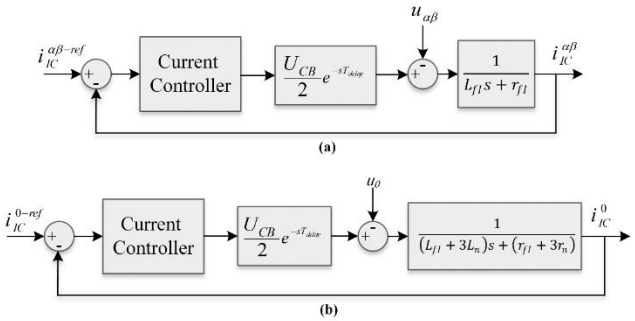


Fig. 10. The dynamic model of the four-leg inverter (a) the model of $\alpha\beta$ axis (b) the model of the 0 axis

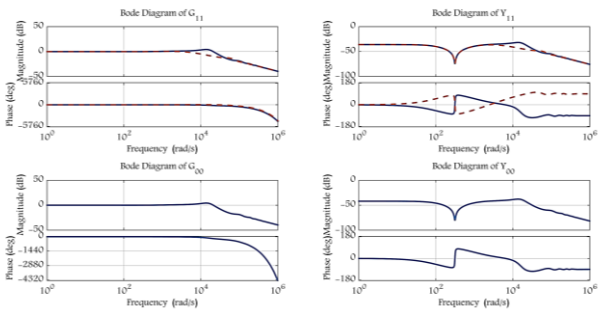


Fig. 11. The frequency response of the Eq. (13), the blue line is related to (+s) and the red line is related to (-s)

Table III

THE CHARACTERISTICS OF THE AC SUBGRID AND THE FOUR-LEG INVERTER

Line-to-line voltage	380 V
The load impedance related to Figs. 13 and 14	$Z_{La}=500\ \Omega \quad Z_{Lb}=3.25+j\,2.2\ \Omega$ $Z_{Lc}=1.55+j1.2\ \Omega$
The impedance of lines	$z_{la}=0.08+j\,0.03\ \Omega \quad z_{lb}=0.05+j\,0.095\ \Omega$ $z_{lc}=0.05+j\,0.19\ \Omega \quad z_{n}=0.04+j\,0.15\ \Omega$
The inductance and resistance of the four-leg inverter	$L_{fl}=6mH \quad r_{fl}=0.02\Omega$ $L_{n}=2mH \quad r_{n}=0.02\Omega$
The maximum value of the effective current of each leg	$I_R=25\ A$
The droop slope of the compensation reference	$m_0=0.001 \quad m_2=0.001$
The characteristics of the current controller of the four-leg inverter	$k_p=0.12 \quad k_i=3.5 \quad \omega_r=6$ $k_{p0}=0.4 \quad k_{i0}=11.66 \quad \omega_{r0}=6$
The switching frequency of the IC	$f_{sw}=10\ kHz$
The complex coefficient	$G+jB=(0.174+j\,0.985)$
PI0 and PI2 controllers	$k_p^0=3 \quad k_i^0=1200 \quad k_p^2=1 \quad k_i^2=1000$
The power transfer range and its control coefficients	$x_T=0.6 \quad x_B=0.8$ $P_T=15000$ $k_a=75000 \quad k_b=75000 \quad k_q=500$

fficients are determined is described in details in [35], [36]. Eq. (13) shows the relationship of the output current:

$$i_{IC}^{\alpha\beta}=G_{11}(\pm s)\times i_{IC}^{\alpha\beta-ref}-Y_{11}(\pm s)\times u^{\alpha\beta} \tag{13-a}$$

$$i_{IC}^{n}=G_{00}(s)\times i_{IC}^{n}-Y_{00}(s)\times u^{n}. \tag{13-b}$$

In Eq. (13), the output currents of the αβ for the currents of positive and zero sequence are represented by +s and for the negative sequence are represented by –s. The frequency response of the transfer function (13) is shown in Fig. 11, considering the data presented in Table III. As seen in this figure, the system bandwidth is wide enough to track the reference currents of positive, negative, and zero sequences.

III. GENERATING THE REFERENCE CURRENT FOR VOLTAGE UNBALANCE COMPENSATION

If the load of the AC subgrid is unbalanced, it will cause an unbalanced current pass through the system and as a result of unbalanced voltage drops in system impedances, the load voltage will also be unbalanced. To compensate the voltage unbalance, the IC could be used as a current source. If the distributed generation source generates a balanced voltage in the AC subgrid (this assumption is true because of the high gain of voltage controller in the control system shown in Fig. 4), Fig.12 can be considered as a model for the AC subgrid and the IC. In this figure, k_0 and k_2 are real or complex coefficients. By applying the electrical circuit rules on the network shown in Fig. 12, the following equation can be written:

$$\mathbf{u}^{abc}-\mathbf{u}_L^{abc}=\mathbf{z}_{ln}\mathbf{i}^{abc} \tag{14}$$

where,

$$\mathbf{x}^{abc}=\begin{bmatrix}x_a & x_b & x_c\end{bmatrix}^T;\quad x=u,i$$

$$\mathbf{u}_L^{abc}=\begin{bmatrix}u_L^a & u_L^b & u_L^c\end{bmatrix}^T$$

$$\mathbf{z}_{ln}=\begin{bmatrix}z_{la}+z_n & z_n & z_n\\ z_n & z_{lb}+z_n & z_n\\ z_n & z_n & z_{lc}+z_n\end{bmatrix}$$

and the superscript T represents the transposed vector. Assuming that injecting a current proportional to the voltages of negative and zero sequences affects the voltages of negative and zero sequences, equations (15) is formed:

$$\begin{bmatrix}u_L^a\\ u_L^b\\ u_L^c\end{bmatrix}=\mathbf{Z}_{load}\begin{bmatrix}i_a+k_0u^0+k_2u^2\\ i_b+k_0u^0+ak_2u^2\\ i_c+k_0u^0+a^2k_2u^2\end{bmatrix} \tag{15}$$

where,

$$\mathbf{Z}_{load}=\begin{bmatrix}Z_{La} & 0 & 0\\ 0 & Z_{Lb} & 0\\ 0 & 0 & Z_{Lc}\end{bmatrix}$$

and $a=1\angle 120^{\circ}$. Using the symmetric components theory [37]:

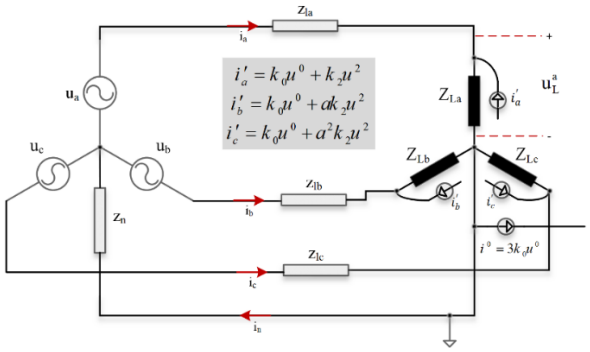


Fig. 12. A model of the AC subgrid, the four-leg inverter, and the unbalanced load

$$\mathbf{u}^{abc} = \mathbf{A}\mathbf{u}^{012}, \quad \mathbf{A} = \begin{bmatrix} 1 & 1 & 1 \\ 1 & a^2 & a \\ 1 & a & a^2 \end{bmatrix}, \quad \mathbf{u}^{012} = \begin{bmatrix} u^0 \\ u^1 \\ u^2 \end{bmatrix} \tag{16}$$

and by substituting the voltages of negative and zero sequences from Eq. (16) into Eq. (15) and (14), the load voltage is calculated as Eq. (17):

$$\mathbf{u}_L^{012} = \mathbf{A}^{-1} \frac{\mathbf{Z}_{load}\mathbf{z}_{ln}^{-1}}{\mathbf{M} + \mathbf{Z}_{load}\mathbf{z}_{ln}^{-1}} \mathbf{A}\mathbf{u}^{012} \tag{17}$$

where,

$$\mathbf{u}^{012} = \begin{bmatrix} 0 & \frac{U_{AC}}{\sqrt{6}} & 0 \end{bmatrix}^T$$

$$\mathbf{M} = \begin{bmatrix} 1 & 0 & 0 \\ 0 & 1 & 0 \\ 0 & 0 & 1 \end{bmatrix} - \frac{k_0}{3}\begin{bmatrix} Z_{La} \\ Z_{Lb} \\ Z_{Lc} \end{bmatrix}\begin{bmatrix} 1 \\ 1 \\ 1 \end{bmatrix}^T - \frac{k_2}{3}\begin{bmatrix} Z_{La} \\ aZ_{Lb} \\ a^2Z_{Lc} \end{bmatrix}\begin{bmatrix} 1 \\ a^2 \\ a \end{bmatrix}^T.$$

Since this network is assumed to be completely asymmetric, therefore the three networks of positive, negative, and zero sequence are related to each other. To understand the relationship between these three networks, the effect of the variations of parameters k_0 and k_2 on voltages of negative, positive, and zero sequences is shown in Fig. 13 for a system with characteristics presented in Table III. It can be seen in Fig. 13 that voltages of negative and zero sequences show less sensitivity to the variations of k_0 and k_2, respectively.

It is worth noting that the coefficients k_0 and k_2 might

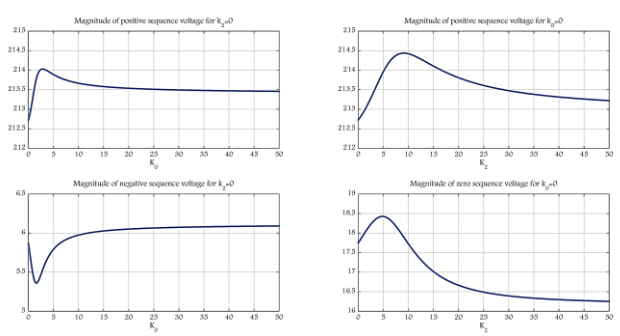


Fig. 13. Variations of positive, negative and zero sequence voltages versus variations of the coefficients k_0 and k_2

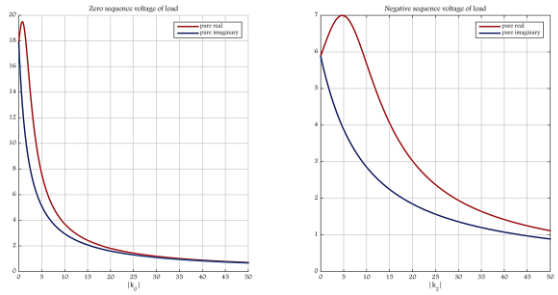


Fig. 14. The effect of real (the red line) and complex (the blue line) k_0 and k_2 coefficients on reduction of zero and negative sequence voltages

be complex. Since the network has an inductive-ohmic nature, the amount of current that flows in the IC could be decreased by selecting an inductive-ohmic admittance (the impedance of which would be capacitive-ohmic). Fig. 14 shows this for pure real and pure imaginary admittances. It is clear from this figure that for equal values of admittance, the imaginary admittance creates greater reduction in the value of the zero and negative sequence voltages. Since the real part of the admittance damps the oscillations in the system, the coefficients k_0 and k_2 are considered to be complex with an angle of 80 degrees.

A. Generating Current Reference

In the proposed scheme, first the sequence components of the voltage of the IC terminal are separated by an adaptive notch filter [38], then the unbalance indices of voltages of zero and negative sequences are calculated using Eq. (18):

$$UF_0 = \frac{u_{rms}^0}{u_{rms}^1}, \quad UF_2 = \frac{u_{rms}^2}{u_{rms}^1}. \tag{18}$$

The error between the values calculated using Eq. (18) and their reference values passes through the PI controller and the magnitudes of the coefficients k_0 and k_2 are obtained. By multiplying these coefficients by the zero and negative sequence voltages and finally multiplying the result into a complex number (G+jB), i'_{abc} and i^0 (shown in Fig. 12) are calculated. Adding up the values of the currents related to the power transfer between subgrids and currents related to the reduction of voltage unbalance creates the reference currents of the four-leg inverter. Furthermore, the reference current of the fourth leg will be i^0. Therefore, by calculating the error between the reference current and the actual current of the converter and applying it to a PR controller, switching signals are generated in a way that the actual current of the converter properly tracks the reference current. Fig. 15 shows the block diagram of the generation of reference current for the four leg inverter in details.

B. Determining the Amount of Voltage Unbalance Compensation

As it was mentioned before, the IC must use its free capacity

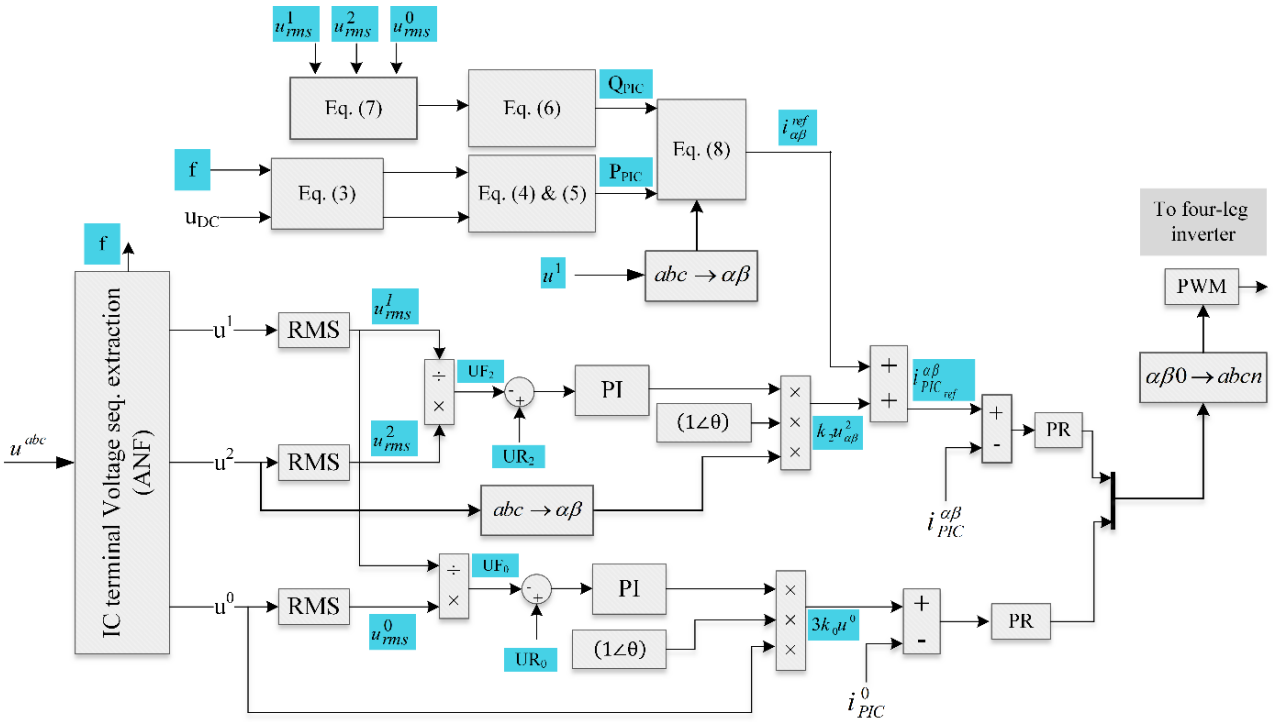


Fig. 15. The block diagram of generating the reference current of the four leg inverter

to provide additional services such as voltage unbalance compensation. On the other hand, the capacity of IC for this task is constantly changing. To avoid overloading the IC and to optimally use the capacity of this converter, these changes must be taken into account in the control system. If the system operates under balanced conditions, the free capacity of the converter could be calculated from its nominal power and the power passing through it. In this paper, in order to avoid overloading the IC, the effective value of the current of each leg has been used for determining the compensation reference (UR_0 & UR_2) such that a greater free capacity causes the unbalance compensation reference to become smaller and consequently the coefficients k_0 and k_2 to increase. Equations (19) and (20) show the way the voltage unbalance compensation reference is determined. Eq. (19) and (20) are obtained considering the fact that the zero sequence current affects all four legs of inverter, while the negative sequence current only affects three legs of inverter. Therefore,

$$\begin{aligned} I_M &= \max\left(i_{IC}^{a-rms}, i_{IC}^{b-rms}, i_{IC}^{c-rms}, i_{IC}^{n-rms}\right) \\ I_N &= \max\left(i_{IC}^{a-rms}, i_{IC}^{b-rms}, i_{IC}^{c-rms}\right) \end{aligned} \tag{19}$$

$$\begin{aligned} UR_0 &= UF_0 - m_0\left(I_R - I_M\right) \\ UR_2 &= UF_2 - m_2\left(I_R - I_N\right) \end{aligned} \tag{20}$$

where *max* is a function for selecting the maximum value between the inputs, m_0 and m_2 are the droop slopes of the unbalance compensation reference value, I_R is the maximum value of the allowed current of each leg, and UR_0 and UR_2 are the compensation references of the negative and zero sequence voltage components.

IV. Simulation Results

In this section, the results of simulation carried out for improving the voltage unbalance on the AC subgrid side of a hybrid microgrid are presented. Simulations are performed for three different cases. In these cases, the capabilities of control scheme in compensating voltage unbalance are fully investigated. A hybrid microgrid as shown in Fig.1 is implemented in MATLAB/Simulink environment. The specifications of the subgrids, line impedances, and controllers are presented in Tables I-III.

A. The First Case

In the first case, in the beginning the load of the AC subgrid is balanced and equal to $P_{L_3ph} = 27^{kVA}\angle 66°$ and the load of the DC subgrid is $P_{L_DC} = 5^{kW}$. Therefore, both subgrids are under under-load conditions. At t=0.7s a single phase load ($P_{L_1ph} = 13^{kW}$) is added to phase *a*. Consequently, the AC subgrid experiences a frequency drop and demands power from the DC subgrid. Furthermore, due to the existence of the single phase load, the AC subgrid voltage becomes unbalanced. At t=1.25s, the voltage unbalance compensation block is activated and tries to compensate the voltage unbalance considering the free capacity of the IC. Simulation results for this case are shown in Fig. 16.

It is clear from Fig. 16 that the amount of the power transferred from the DC subgrid to the AC subgrid is equal to 5.5 kW. Moreover, the ratios of the negative and zero sequence

voltages to the positive sequence voltage have been decreased from 0.8% to 0.3% and from 4% to 2.2%, respectively and as a result, the effective value of phase voltages have also been modified. This is due to the decrease in the amount of the unbalance in the current drawn from the source of AC subgrid. As can be seen from Fig. 16, the voltage oscillations of DC subgrid are very low due to the difference in DC and AC subgrid voltage levels. In fact, the active power oscillations created by the unbalanced voltage compensation have affected voltage of C_B. As a result of the presence of a buck/boost converter, these oscillations do not have a significant effect on DC subgrid voltage. In fact, the buck/boost converter acts as an operator which improve voltage quality of the DC subgrid. If the maximum allowable current of the four-leg inverter increases, the voltage unbalance percentage decreases even more. This is shown in Fig. 17 by doubling the maximum allowable current.

B. The Second Case

In the second case, a single load phase, $P_{L_1ph} = 15^{kW}$, is connected to phase *a* and a load of $P_{L_2ph} = 11.2^{kVA}\angle 26°$ is connected between phases *a* and *c* of the AC subgrid. A load of $P_{L_DC} = 5^{kW}$ is connected to the DC subgrid. At t=0.7s the load $P_{L_DC} = 30^{kW}$ enters the circuit. Therefore, the DC subgrid demands power from the AC subgrid which has unbalanced load. The amount of power transferred from the AC subgrid to the DC subgrid is equal to 8^{kW} as shown in Fig. 18. At t=1.25s, the voltage unbalance compensation block is activated and the ratios of the negative and zero sequence voltages to the positive sequence voltage are decreased from 1.7% to 1.2% and from 5% to 3.1%, respectively. Simulation results are shown in Fig. 18.

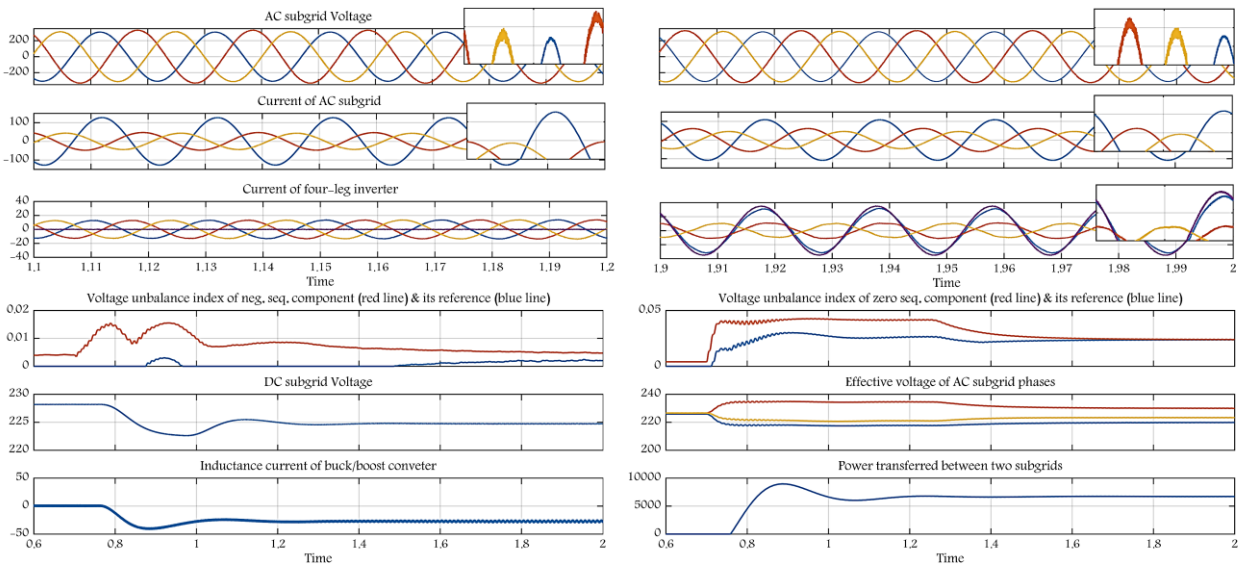


Fig. 16. Simulation results of the first case

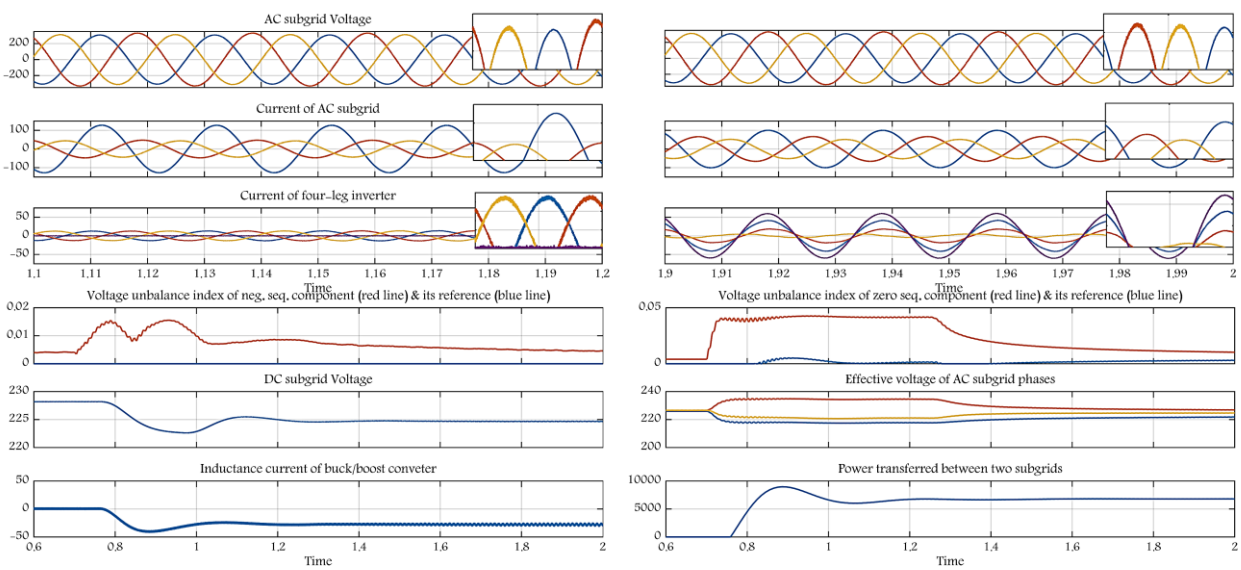


Fig. 17. Simulation results of the first case with a maximum current of 50 A for four-leg inverter

C. The Third Case

In the third case, both subgrids are under conditions that none of them has extra power to transfer to the other. The AC subgrid has a balanced load of $P_{L_3ph} = 27^{kVA}\angle 66°$, a single of $P_{L_1ph} = 10^{kW}$ in phase a, and a load of $P_{L_2ph} = 9.5^{kVA}\angle 32°$ between phases a and c. The DC subgrid supplies a load of $P_{L_DC} = 40^{kW}$. At t=1.25, the voltage unbalance compensation block is activated and the ratios of zero and negative sequence voltages to the positive sequence voltage are decreased from 1.5% to 0.05% and from 4% to 2%, respectively. Under such condition, during the first half-cycle the IC receives the power required for compensating voltage unbalance, and during the next half-cycle it returns this power back to the subgrid. This is clearly observed in the current of the buck/boost converter. Of course some power is dissipated under such conditions that must be supplied by both subgrids. Fig. 19 shows the simulation results of this case.

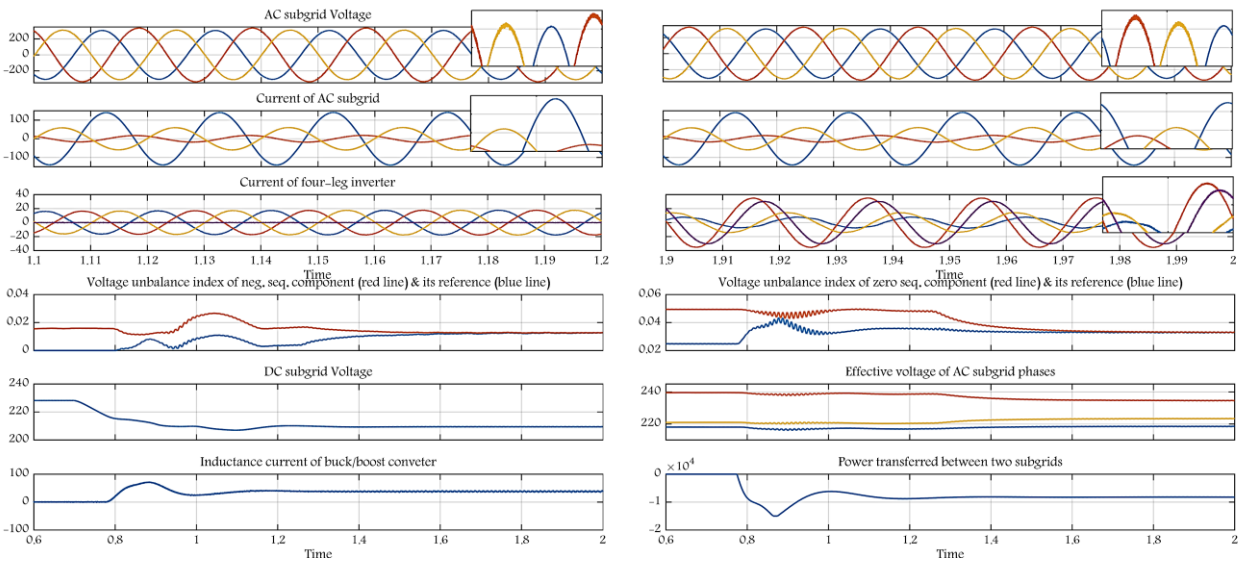


Fig. 18. Simulation results of the second case

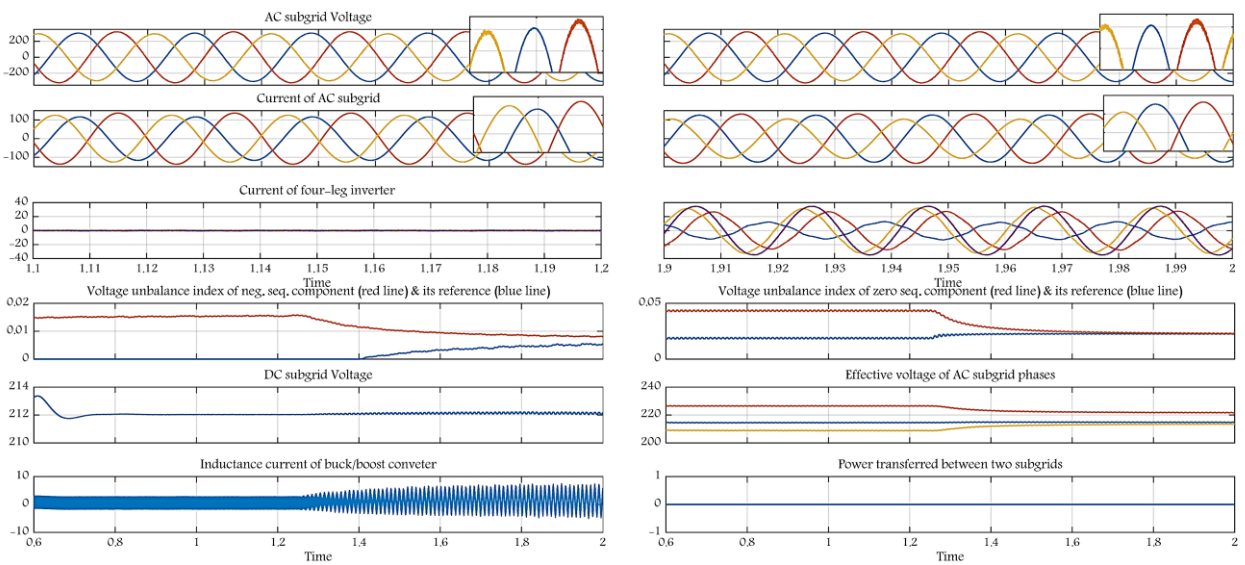


Fig. 19. Simulation results of the third case

V. Conclusion

In this paper, using the free capacity of the IC in the hybrid microgrid made it possible to decrease the voltage unbalance on the AC subgrid side. This is carried out by injecting a current proportional to the negative and zero sequence voltages. The IC acts as a controlled current source, therefore the capacity of the converter must be taken into consideration in the amount of its injected current. In this paper, the value of the voltage unbalance compensation reference is determined in a floating manner in proportion to the effective value of the

current of each leg of the converter. On the other hand, to optimally use the capacity of IC, the injected currents are considered to be leading with respect to the zero and negative sequences. Consequently, the IC does its best to decrease the voltage unbalance considering its free capacity.

REFERENCES

[1] *IEEE Guide for Design, Operation, and Integration of Distributed Resource Island Systems with Electric Power Systems*, IEEE Std. 1547.4-2011,, 2011.

[2] T. Vigneysh, N. Kumarappan, and R. Arulraj, "Operation and control of wind/fuel cell based hybrid microgrid in grid connected mode," *Automation, Computing, Communication, Control and Compressed Sensing (iMac4s), 2013 International Multi-Conference on*, pp. 754-758, 2013.

[3] R. Noroozian and G. B. Gharehpetian, "Combined operation of converter-based distributed generation unit in DC distribution system in order to have premium power quality," *European Transactions on Electrical Power*, vol. 22, no. 4, pp. 449-470, 2012.

[4] Q. Shafiee, J. M. Guerrero, and J. C. Vasquez, "Distributed secondary control for islanded microgrids—A novel approach," *IEEE Transactions on power electronics*, vol. 29, no. 2, pp. 1018-1031, 2014.

[5] Y. Jafarian, A. Karimi, and H. Bevrani, "Secondary Voltage Control in a Hybrid Microgrid," *International Journal of Industrial Electronics, Control and Optimization*, vol. 2, no. 3, pp. 221-232, 2019.

[6] H. Karimi, H. Nikkhajoei, and R. Iravani, "Control of an electronically-coupled distributed resource unit subsequent to an islanding event," *IEEE Transactions on Power Delivery*, vol. 23, no. 1, pp. 493-501, 2008.

[7] B. Kroposki, R. Lasseter, T. Ise, S. Morozumi, S. Papathanassiou, and N. Hatziargyriou, "Making microgrids work," *IEEE Power and Energy Magazine*, vol. 6, no. 3, pp. 40-53, 2008.

[8] J. M. Guerrero, J. C. Vasquez, J. Matas, L. G. De Vicuña, and M. Castilla, "Hierarchical control of droop-controlled AC and DC microgrids—A general approach toward standardization," *IEEE Transactions on Industrial Electronics*, vol. 58, no. 1, pp. 158-172, 2011.

[9] S. Bahramirad, W. Reder, and A. Khodaei, "Reliability-constrained optimal sizing of energy storage system in a microgrid," *IEEE Transactions on Smart Grid*, vol. 3, no. 4, pp. 2056-2062, 2012.

[10] A. Gupta, S. Doolla, and K. Chatterjee, "Hybrid AC–DC microgrid: systematic evaluation of control strategies," *IEEE Transactions on Smart Grid*, vol. 9, no. 4, pp. 3830-3843, 2018.

[11] P. C. Loh, D. Li, Y. K. Chai, and F. Blaabjerg, "Hybrid AC–DC microgrids with energy storages and progressive energy flow tuning," *IEEE transactions on power electronics*, vol. 28, no. 4, pp. 1533-1543, 2013.

[12] X. Liu, P. Wang, and P. C. Loh, "A hybrid AC/DC microgrid and its coordination control," *IEEE Transactions on Smart Grid*, vol. 2, no. 2, pp. 278-286, 2011.

[13] F. Nejabatkhah and Y. W. Li, "Overview of power management strategies of hybrid AC/DC microgrid," *IEEE Transactions on Power Electronics*, vol. 30, no. 12, pp. 7072-7089, 2015.

[14] P. C. Loh, D. Li, Y. K. Chai, and F. Blaabjerg, "Autonomous operation of ac-dc microgrids with minimised interlinking energy flow," *IET Power Electronics*, vol. 6, no. 8, pp. 1650-1657, 2013.

[15] R. Ghanizadeh, M. Ebadian, and G. B. Gharehpetian, "Non-linear load sharing and voltage harmonics compensation in islanded microgrids with converter interfaced units," *International Transactions on Electrical Energy Systems*, vol. 27, no. 1, pp. e2237, 2017.

[16] E. Fuchs and M. A. Masoum, *Power quality in power systems and electrical machines*: Academic press, 2011.

[17] B. Nanda and R. Jena, "Power Quality Analysis by using Active Filter in AC/DC Microgrid," *International Journal of Scientific Research in Science and Technology (IJSRST)*, vol. 4, no. 9, pp. 47-56, 2018.

[18] L. F. Monteiro, M. Aredes, C. Couto, and J. L. Afonso, "Control algorithms for a unified power quality conditioner based on three-level converters," *International Transactions on Electrical Energy Systems*, vol. 25, no. 10, pp. 2394-2411, 2015.

[19] T. XiangQian, X. Keqing, S. Ming, and M. Xianhong, "Reactive power and unbalance compensation with DSTATCOM," *International Conference on Electrical Machines and Systems*, pp. 1181-1184, 2005.

[20] F. Nejabatkhah, Y. W. Li, and B. Wu, "Control strategies of three-phase distributed generation inverters for grid unbalanced voltage compensation," *IEEE Transactions on Power Electronics*, vol. 31, no. 7, pp. 5228-5241, 2016.

[21] M. Savaghebi, A. Jalilian, J. C. Vasquez, and J. M. Guerrero, "Autonomous voltage unbalance compensation in an islanded droop-controlled microgrid," *IEEE Transactions on Industrial Electronics*, vol. 60, no. 4, pp. 1390-1402, 2012.

[22] L. Meng, X. Zhao, F. Tang, M. Savaghebi, T. Dragicevic, J. C. Vasquez, *et al.*, "Distributed voltage unbalance compensation in islanded microgrids by using a dynamic consensus algorithm," *IEEE Transactions on Power Electronics*, vol. 31, no. 1, pp. 827-838, 2015.

[23] S. D. Dehnavi and E. Shayani, "Compensation of Voltage disturbances in hybrid AC/DC Microgrids using series converter," *Ciência e Natura*, vol. 37, no. 2, pp. 349-356, 2015.

[24] P. G. Khorasani, M. Joorabian, and S. G. Seifosadat, "A new proposal for the design of hybrid AC/DC microgrids toward high power quality," *Turkish Journal of Electrical Engineering & Computer Sciences*, vol. 25, no. 5, pp. 4033-4049, 2017.

[25] K. Sun, X. Wang, Y. W. Li, F. Nejabatkhah, Y. Mei, and X. Lu, "Parallel operation of bidirectional interfacing converters in a hybrid AC/DC microgrid under unbalanced grid voltage conditions," *IEEE Transactions on Power Electronics*, vol. 32, no. 3, pp. 1872-1884, 2016.

[26] F. Nejabatkhah, Y. W. Li, K. Sun, and R. Zhang, "Active power oscillation cancelation with peak current sharing in parallel interfacing converters under unbalanced voltage," *IEEE Transactions on Power Electronics*, vol. 33, no. 12, pp. 10200-10214, 2018.

[27] P. C. Loh, D. Li, Y. K. Chai, and F. Blaabjerg, "Autonomous control of interlinking converter with energy storage in hybrid AC–DC microgrid," *IEEE Transactions on Industry Applications*, vol. 49, no. 3, pp. 1374-1382, 2013.

[28] P. Wang, C. Jin, D. Zhu, Y. Tang, P. C. Loh, and F. H. Choo, "Distributed control for autonomous operation of a three-port AC/DC/DS hybrid microgrid," *IEEE*

Transactions on Industrial Electronics, vol. 62, no. 2, pp. 1279-1290, 2015.

[29] J. M. Guerrero, J. C. Vasquez, J. Matas, M. Castilla, and L. G. de Vicuña, "Control strategy for flexible microgrid based on parallel line-interactive UPS systems," *IEEE Transactions on Industrial Electronics*, vol. 56, no. 3, pp. 726-736, 2009.

[30] J. Zhang, D. Guo, F. Wang, Y. Zuo, and H. Zhang, "Control strategy of interlinking converter in hybrid AC/DC microgrid," *International Conference on Renewable Energy Research and Applications (ICRERA)*, pp. 97-102, 2013.

[31] P. C. Loh, D. Li, Y. K. Chai, and F. Blaabjerg, "Autonomous operation of hybrid microgrid with AC and DC subgrids," *IEEE transactions on power electronics*, vol. 28, no. 5, pp. 2214-2223, 2012.

[32] *IEEE standard definitions for the measurement of electric power quantities under sinusoidal, nonsinusoidal, balanced, or unbalanced conditions*, IEEE Std. 1459-2010, 2010.

[33] B. Johansson, "Improved models for DC-DC converters," Dept. Ind. Electr. Eng. Autom., Lund University, sweden, 2003.

[34] P. A. F. Galarza, "Stationary frame control of three-leg and four-leg voltage source inverters in power system applications: Modelling and simulations," M.S. Thesis, The University of Nottingham, 2016.

[35] D. G. Holmes, T. A. Lipo, B. P. Mcgrath, and W. Y. Kong, "Optimized design of stationary frame three phase AC current regulators," *IEEE transactions on power electronics*, vol. 24, no. 11, pp. 2417-2426, 2009.

[36] S. H. Tabatabaei, M. M. BAJESTAN, and A. Jalilian, "Shunt active power filter control for compensating current power quality problems in three-phase three-wire systems based on an adaptive notch filter," *Turkish Journal of Electrical Engineering & Computer Sciences*, vol. 24, no. 4, pp. 2539-2555, 2016.

[37] A. Bergen and V. Vittal, *Power systems analysis*, *Prentice Hall*, 2000.

[38] D. Yazdani, M. Mojiri, A. Bakhshai, and G. Joós, "A fast and accurate synchronization technique for extraction of symmetrical components," *IEEE Transactions on Power Electronics*, vol. 24, no. 3, pp. 674-684, 2009.



Seyed Hossein Tabatabaei was born in Gonbad Kavous, Iran, in 1987. He received the B.Sc. degree from the Hakim Sabzevari University, Sabzevar, Iran, in 2010, the M.Sc. degree in electrical engineering from the Iran University of Science & Technology (IUST), Tehran, Iran, in 2013. He is currently a Ph.D. student of Electrical Engineering in university of Birjand, Iran. His research interests are renewable energy, power electronics and power quality.



Hussein Eliasi received the B.S. degree in electrical engineering from the Ferdowsi University of Mashhad (FUM), Iran, in 2001. He received the M.S. and the Ph.D. degrees from Amirkabir University of technology (Tehran), Iran, in 2005 and 2011, respectively. He is currently an assistance professor in faculty of electrical engineering at University of Birjand, Iran. His research interests include Constrained Nonlinear Dynamics Systems, Robust Control, Parameter Optimization of Model Predictive Control, Transient Stability in Power Systems and Load Following by Nuclear Power Plants.



Hamid Reza Najafi was born in Mashhad, Iran, on July 9, 1960. He received the B.Sc. and the M.Sc degrees in Electrical Engineering from Ferdowsi University (Mashhad, Iran) in 1986 and 1991 and the Ph.D. degree from Iran University of Science and Technology (IUST), Tehran, Iran, 2004, all in Electrical Engineering-POWER. He is Associate Professor at electrical engineering department of University of Birjand, Iran. He is a member of IEEE.

IECO

This page intentionally left blank.